Density Functional Theory/GIAO Studies of the ^{13}C, ^{15}N, and ^{1}H NMR Chemical Shifts in Aminopyrimidines and Aminobenzenes: Relationships to Electron Densities and Amine Group Orientations

Michael Barfield* and Paul Fagerness†

Contribution from the Department of Chemistry, University of Arizona, Tucson, Arizona 85721, and Drug Metabolism Research, Pharmacia and Upjohn Incorporated, Kalamazoo, Michigan 49001

Received March 28, 1997. Revised Manuscript Received June 23, 1997⊗

Abstract: The dependence of the ^{13}C, ^{15}N, and ^{1}H isotropic NMR chemical shifts on amine substitution of aromatic ring systems are examined both experimentally and by DFT/GIAO (density functional theory/gauge including atomic orbitals) methods. There are large, monotonic decreases in the chemical shifts at odd-numbered (*ortho* and *para*) pyrimidine ring positions which do not occur at the even-numbered (*ipso* and *meta*) atoms as amine groups progressively replace hydrogens at the latter positions. This behavior parallels the computed $2p_z$ electron densities which for the pyrimidine series increase monotonically at N1, N3, and C5 but exhibit small changes at the C2, C4, and C6 positions. Identical trends are noted for the aminobenzenes. The ring atom chemical shifts and $2p_z$ electron densities at *ortho* and *para* (but not *meta*) positions are quite sensitive to the orientations of the amine groups which are pyramidalized as the result of balance between delocalization with the ring and the use of strongly directed sp^3 orbitals at the nitrogen. The calculated results show that the barriers to amine group torsional and inversion motions are low, but averaging the chemical shifts over these appears to be relatively unimportant. Differences between the DFT and Hartree−Fock-based chemical shifts show that electron correlation effects monotonically increase with the number of NH_2 substituents.

I. Introduction

Presented here is an extensive experimental and theoretical study of NMR magnetic shielding spectra of the aminopyrimidines **2, 4, 5,** and **8**−**12**, benzene (**1**), and the series of aminobenzenes **3**, **6**, and **7**. Progressive replacement of

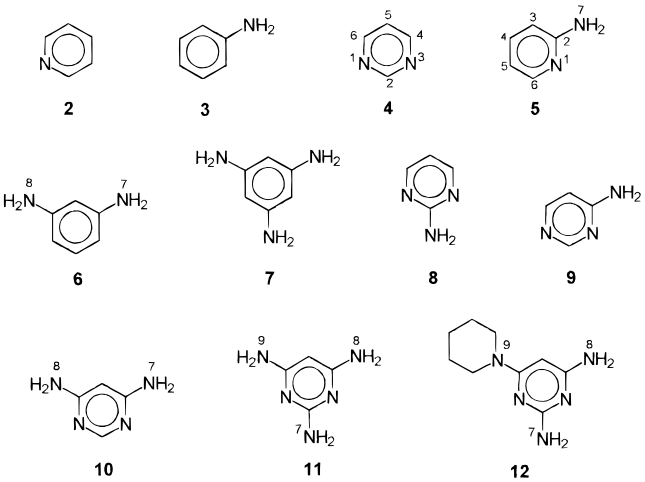

hydrogens by amine groups at the even-numbered pyrimidine carbons leads to compounds that have potent pharmacological activity. In fact, the last member of this series (**12**) is the desoxy form of Minoxidil, an antihypertensive agent (Loniten) and a topical hair regrowth stimulant (Rogaine). Among the aromatic carbons and nitrogens in this series of compounds the chemical shift ranges are 90 and 140 ppm, respectively. Since these represent large fractions of the total shift ranges for these two nuclei, the changes in electronic structures should also be large. Indeed, one of the earliest NMR correlations was that between ^{1}H and ^{13}C NMR chemical shifts and π-electron densities of aromatic and heteroaromatic systems.[1,2] This was a puzzle in the early studies of aromatic molecules because changes in the diamagnetic term are small, while changes in the paramagnetic term should be in the opposite direction. The theoretical basis for the correlations was addressed by several groups.[3−6]

The ^{1}H, ^{13}C, and ^{15}N NMR chemical shifts of nitrogen heterocyclic compounds have been the subject of a number of experimental and theoretical studies.[7−9] There have also been a number of NMR studies of chemical shifts in aminobenzenes[10,11] and aminopyrimidines.[12−17] An important aspect of magnetic shielding in amine-substituted aromatic compounds,

† Pharmacia and Upjohn Inc.

⊗ Abstract published in *Advance ACS Abstracts,* September 1, 1997.

(1) Spiesecke, H.; Schneider, W. G. *Tetrahedron Lett.* **1961**, 468−472. Spiesecke, H.; Schneider, W. G. *J. Chem. Phys.* **1961**, *35*, 731−738.
(2) Lauterbur, P. C. *J. Am. Chem. Soc.* **1961**, *83*, 1838−1846. Lauterbur, P. C. *J. Chem. Phys.* **1965**, *43*, 360−363.
(3) Karplus, M.; Pople, J. A. *J. Chem. Phys.* **1963**, *38*, 2803−2807.
(4) Alger, T. D.; Grant, D. M.; Paul, E. G. *J. Am. Chem. Soc.* **1966**, *88*, 5397−5406.
(5) Tokuhiro, T.; Wilson, N. K.; Fraenkel, G. *J. Am. Chem. Soc.* **1968**, *90*, 3622−3628.
(6) Tokuhiro, T.; Fraenkel, G. *J. Am. Chem. Soc.* **1969**, *91*, 5005−5013.
(7) Batterham, T. J. *NMR Spectra of Simple Heterocycles*; Wiley: New York, 1973.
(8) Pugmire, R. J.; Grant, D. M. *J. Am. Chem. Soc.* **1968**, *90*, 697−706. Pugmire, R. J.; Grant, D. M. *J. Am. Chem. Soc.* **1968**, *90*, 4232−4238.
(9) Schindler, M. *J. Am. Chem. Soc.* **1987**, *109*, 5950−5955. Schindler, M. *J. Am. Chem. Soc.* **1988**, *110*, 6623−6630. Schindler, M. *Magn. Reson. Chem.* **1988**, *26*, 394−407.
(10) Yamazaki, M.; Usami, T.; Takeuchi, T. *Nippon Kagaku Kaishi* **1973**, 2135−2141.
(11) Dorie, J.; Mechin, B.; Martin, G. *Org. Magn. Reson.* **1979**, *12*, 229−234.
(12) Riand, J.; Chenon, M. T.; Lumbroso-Bader, N. *Tetrahedron Lett.* **1974**, 3123−3126.

S0002-7863(97)00990-6 CCC: $14.00

which appears not to have been addressed in previous NMR studies, is the dependence of NMR chemical shifts on amine group orientations. Experimental and theoretical studies of amine substituted aromatic compounds show that the amine group hydrogens are out of the plane by an amount which depends on a balance between π-electron delocalization across the C−N bond and the tendency of the amine group to form strongly directed sp^3-hybridized orbitals.[18−25] There are relatively few structural studies among these compounds because of spectral complexity arising from multiple, large-amplitude vibrations[26] associated with low NH_2 torsion and inversion barriers.

Computational methods for calculating magnetic shielding, especially those based on distributed origins algorithms, have continued to improve.[27] The GIAO (gauge including atomic orbital) method,[28] which was used for magnetic shielding studies by Ditchfield,[29] is now widely used in efficient implementations.[30] The IGLO[31,32] (individual gauge for localized orbitals) and LORG[33] (local orbitals−local origins) algorithms also provide satisfactory magnetic shielding results using modest basis sets. More recently, all three methods have been extended to include electron correlation effects, which are especially important for unsaturated and aromatic systems.[34−39] The introduction of density functional theory (DFT) for calculations of magnetic shielding[40−44] greatly extends the size of molecules which can be examined with inclusion of electron correlation effects.

Presented here are experimental and calculated ^{13}C, ^{15}N, and ^{1}H isotropic NMR chemical shifts for benzene (**1**), pyridine (**2**), aniline (**3**), pyrimidine (**4**), 2-aminopyridine (**5**), 1,3-diaminobenzene (**6**), 1,3,5-triaminobenzene (**7**), 2-aminopyrimidine (**8**), 4-aminopyrimidine (**9**), 4,6-diaminopyrimidine (**10**), 2,4,6-triaminopyrimidine (**11**), and 2,4-diamino-6-(1-piperidinyl)-pyrimidine (desoxyminoxidil) (**12**). The computational methods for molecular structures and magnetic shielding are presented in the next section. The experimental details are given in section III. Section IV follows with comparisons of the calculated ^{13}C, ^{15}N, and ^{1}H NMR chemical shifts with the experimental data. In section V, it is shown that the experimental and calculated ring carbon chemical shifts follow a dependence on substitution patterns similar to those for the $2p_z$ electron densities. In section VI, the chemical shifts and electron densities for three model compounds are found to be quite sensitive to NH_2 orientation.

II. Computational Details

A. Molecular Structures. Good quality shielding results (especially for molecules with heteroatoms) depend on the quality of the basis sets and the structural data. Since accurate experimental data are seldom available for the molecules of interest, energy optimized geometries are frequently used.[45] Previous studies of amine group orientations have demonstrated

(13) Turner, C. J.; Cheeseman, G. W. H. *Org. Magn. Reson.* **1976**, *8*, 357−360.
(14) Retcofsky, H. L.; Friedel, R. A. *J. Phys. Chem.*, **1978**, *72*, 2619−2622.
(15) Riand, J.; Chenon, M. T.; Lumbroso-Bader, N. *Org. Magn. Reson.* **1977**, *9*, 572−579.
(16) Cheeseman, G. W. H.; Turner, C. J.; Brown, D. J. *Org. Magn. Reson.* **1979**, *12*, 212−215.
(17) Städeli, W.; von Philipsborn, W.; Wick, A.; Kompis, I. *Helv. Chim. Acta* **1980**, *63*, 504−522.
(18) Lister, D. G.; Tyler, J. K.; Høg, J. H.; Larsen, N. W. *J. Mol. Struct*. **1974**, *23*, 253−264.
(19) Fukuyo, M.; Hirotsu, K.; Higuchi, T. *Acta Crystallogr. B.* **1982**, *38*, 640−643.
(20) Riggs, N. V.; Radom, L. *Int. J. Quantum Chem.* **1987**, *31*, 393−403. Riggs, N. V. *Chem. Phys. Lett.* **1991**, *177*, 447−450.
(21) Wang, Y.; Saebø, S.; Pittman, C. U.,Jr. *THEOCHEM* **1993**, *100*, 91−98.
(22) Kydd, R. A.; Mills, I. M., *J. Mol. Spectrosc.* **1972**, *42*, 320−326. Christen, D.; Norbury, D.; Lister, D. G.; Palmieri, P. *Faraday Trans. 2*, **1975**, 438−446.
(23) Boggs, J. E.; Niu, Z. *J. Comput. Chem.* **1985**, *6*, 46−55. Smith, D. A.; Ulmer, C. W., III; Gilbert, M. J. *J. Comput. Chem.* **1992**, *13*, 640−650.
(24) Sponer, J.; Hobza, P. *J. Phys. Chem.* **1994**, *98*, 3161−3164. Sponer, J.; Hobza, P. *J. Am. Chem. Soc.* **1994**, *116*, 709−714. Sponer, J.; Hobza, P. *Int. J. Quantum Chem.* **1996**, *57*, 959−970.
(25) Sulzbach, H. M.: Schleyer, P. v. R.; Schaefer, H. F., III *J. Am. Chem. Soc.* **1995**, *117*, 2632−37.
(26) Wilson, E. B. *J. Chem. Phys.* **1938**, *6*, 740−745. Longuet-Higgins, H. C. *Mol. Phys.* **1963**, *6*, 445−460. Hougen, J. T.; Bunker, P. R.; Johns, J. W. C. *J. Mol. Spectrosc.* **1970**, *34*, 136−172. Hougen, J. T. *J. Phys. Chem.* **1986**, *90*, 562−568. Hollas, J. M. *Chem. Soc. Rev.* **1993**, *22*, 371−382. Csonka, G. I.; Sztraka, L. *Chem. Phys. Lett.* **1995**, *233*, 611−618.
(27) For general reviews of theory of magnetic shielding see, for example: Jameson, C. J. In *Nuclear Magnetic Resonance*; Specialist Periodical Reports; The Chemical Society: London, 1995; no. 24 and previous chapters in this series. Chesnut, D. B. *Annu. Rep. NMR Spectrosc.* **1994**, *29*, 71−122. Webb, G. A. In *NMR Shieldings and Molecular Structure*; Tossell, J. A., Ed.; Kluwer Academic Publishers: Norwell, MA, 1993.
(28) London, F. *J. Phys. Radium (Paris)* **1937**, *8*, 397−409.
(29) Ditchfield, R. *Mol. Phys.* **1974**, *27*, 789−807.
(30) Wolinski, K.; Hinton, J. F.; Pulay, P. *J. Am. Chem. Soc.* **1990**, *112*, 8251−8260. Häser, M.; Ahlrichs, R.; Baron, H. P.; Weiss, P.; Horn, H. *Theor. Chim. Acta* **1992**, *83*, 455−470.
(31) Kutzelnigg, W. *Isr. J. Chem.* **1980**, *19*, 193−200. Schindler, M.; Kutzelnigg, W. *J. Chem. Phys.* **1982**, *76*, 1919−1933. Schindler, M.; Kutzelnigg, W. *J. Am. Chem. Soc.* **1983**, *105*, 1360−1370. Schindler, M.; Kutzelnigg, W. *Mol. Phys.* **1983**, *48*, 781−798.
(32) For reviews, see: Kutzelnigg, W.; Fleischer, U.; Schindler, M. In *NMR Basic Principles and Progress*; Diehl, P., Fluck, E., Kosfeld, R., Eds.; Springer: Berlin, 1990; Vol. 23, pp 165−262. Kutzelnigg, W.; van Wüllen, Ch.; Fleischer, U.; Franke, R.; Mourik, T. v. In *NMR Shieldings and Molecular Structure*; Tossell, J. A. Ed.: Kluwer Academic Publishers: Norwell, MA, 1993.
(33) Hansen, Aa. E.; Bouman, T. D. *J. Chem. Phys.* **1985**, *82*, 5035−5047. Facelli, J. C.; Grant, D. M.; Bouman, T. D.; Hansen, Aa. E. *J. Comput. Chem.* **1990**, *11*, 32−44. Kirby, R. A.; Hansen, Aa. E. *Int. J. Quantum Chem.* **1996**, *57*, 199−205.
(34) Bouman, T. D.; Hansen, Aa. E. *Chem. Phys. Lett.* **1990**, *175*, 292−299. Bouman, T. D.; Hansen, Aa.E. *Chem. Phys. Lett.* **1992**, *197*, 59−66.
(35) Oddershede, J.; Geertsen, J. *J. Chem. Phys.* **1990**, *92*, 6036−6042.
(36) Gauss, J. *Chem. Phys. Lett.* **1992**, *191*, 614−620. Gauss, J. *J. Chem. Phys.* **1993**, *99*, 3629−3643. Bühl, M.; Gauss, J.; Hofmann, M.; Schleyer, P. v. R. *J. Am. Chem. Soc.* **1993**, *115*, 12385−12390. Bühl, M.; Thiel, W.; Fleischer, U.; Kutzelnigg, W. *J. Phys. Chem.* **1995**, *99*, 4000−4007.
(37) Cybulski, S. M.; Bishop, D. M. *J. Chem. Phys.* **1993**, *98*, 8057−8064.
(38) Sundholm, D.; Gauss, J.; Ahlrichs, R. *Chem. Phys. Lett.* **1995**, *243*, 264−268. Gauss, J.; Stanton, J. F. *J. Chem. Phys.* **1996**, *103*, 3561−3577. Gauss, J.; Stanton, J. F. *J. Chem. Phys.* **1996**, *104*, 2574−2583.
(39) van Wüllen, C.; Kutzelnigg, W. *J. Chem. Phys.* **1996**, *104*, 2330−2340.
(40) Malkin, V. G.; Malkina, O. L.; Salahub, D. R. *Chem. Phys. Lett.* **1993**, *204*, 87−95. Malkin, V. G.; Malkina, O. L.; Casida, M. E.; Salahub, D. R. *J. Am. Chem. Soc.* **1994**, *116*, 5898−5908. Kaupp, M.; Malkin, V. G.; Malkina, O. L.; Salahub, D. R. *Chem. Phys. Lett.* **1995**, *235*, 382−388. Kaupp, M.; Malkin, V. G.; Malkina, O. L.; Salahub, D. R. *J. Am. Chem. Soc.* **1995**, *117*, 1851−1852. Malkin, V. G.; Malkina, O. L.; Salahub, D. R. *J. Am. Chem. Soc.* **1995**, *117*, 3294−3295. Woolf, T. B.; Malkin, V. G.; Roux, B.; Malkina, O. L.; Salahub, D. R. *Chem. Phys. Lett.* **1995**, *239*, 186−194.
(41) van Wüllen, C. *J. Chem. Phys.* **1995**, *102*, 2806−2811. Malkin, V. G.; Malkina, O. L.; Salahub, D. R. *J. Chem. Phys.* **1996**, *104*, 1163−1164. van Wüllen, C. *J. Chem. Phys.* **1996**, *104*, 1165.
(42) Schreckenbach, G.; Ziegler, T. *J. Phys. Chem.* **1995**, *99*, 606−611. Ruiz-Morales, Y.; Schreckenbach, G.; Ziegler, T. *J. Phys. Chem.* **1996**, *100*, 3359−3367. Schreckenbach, G.; Ruiz-Morales, Y.; Ziegler, T. *J. Chem. Phys.* **1996**, *104*, 8605−8612.
(43) Cheeseman, J. R.; Trucks, G. W.; Keith, T. A.; Frisch, M. J. *J. Chem. Phys.***1996**, *104*, 5497−5509.
(44) Gaussian 94, Revision B.3; Frisch, M. J.; Trucks, G. W.; Schlegel, H. B.; Gill, P. M. W.; Johnson, B. G.; Robb, M. A.; Cheeseman, J. R.; Keith, T. G.; Petersson, A.; Montgomery, J. A.; Raghavachari, K.; Al-Laham, M. A.; Zakrzewski, V. G.; Ortiz, J. V.; Foresman, J. B.; Peng, C. Y.; Ayala, P. Y.; Chen, W.; Wong, M. W.; Andres, J. L.; Replogle, E. S.; Gomperts, R.; Martin, R. L.; Fox, D. J.; Binkley, J. S.; Defrees, D. J.; Baker, J.; Stewart, J. P.; Head-Gordon, M.; Gonzalez, C.; Pople, J. A. Gaussian, Inc.: Pittsburgh, PA, 1995.
(45) Bühl, M.; Schleyer, P. v. R. *J. Am. Chem. Soc.* **1992**, *114*, 477−491.

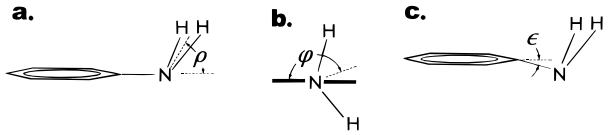

Figure 1. (a) The amine group inversion coordinate ρ is defined as the angle between the H−N−H bisector and the extension of the C−N bond. (b) The torsion angle φ is the dihedral angle between the bisector of the H−N−H group and the average plane of the ring. (c) The angle ϵ is defined as the angle between the C−N bond the bisector of ring atoms X−C−X.

the importance of including electron correlation effects.[24,25] Since polarization functions on hydrogens appear to be a less important factor, these were not included here in geometry optimizations.[24] All molecular geometries are fully optimized (subject to molecular symmetry) using the Gaussian 94 codes[44] with triple split valence basis sets and polarization functions[46] both at the MP2/6-311G* level of Møller−Plesset perturbation theory[47] and the BPW91/6-311G* level of density functional theory.[48−53] The latter method uses the Becke-88 exchange functional[50,51] with the gradient-correlated Perdew−Wang 1991 correlation functional.[52] Structures for desoxyminoxidil (**12**), the largest molecule investigated in this series, were obtained at the split valence MP2/6-31G* and the BPW91/6-31G* levels. The frozen core approximation was used for MP2 calculations, wherein the innershell electron of the carbon and nitrogen atoms were not included in the calculations of electron correlation energies.

Of particular interest in this study was the investigation of the importance of amine group pyramidalization to the calculated chemical shifts. The amine group orientation is specified by two angles. The inversion coordinate ρ is defined as the angle between the H−N−H bisector and the extension of the C−N bond as depicted in Figure 1a. The torsion angle φ in Figure 1b is the dihedral angle between the bisector of the H−N−H group and the plane formed by the ring *ipso* and two *ortho* atoms. Thus, the planar arrangement of the amine group corresponds to $\varphi = 90°$ and $\rho = 0°$. For symmetrical NH_2 orientations, such as those in aniline, the global minimum occurs for $\varphi_e = 90°$. The X-ray data for aniline and energy-optimized structures for all nonplanar aromatic amines show that the C−N bond dips slightly below the aromatic plane as depicted in Figure 1c. The angle ϵ is here defined as the angle between the Ci−N bond and the bisector of the ring atoms X−Ci−X. The calculated results for the equilibrium geometries indicate the latter are typically in the range 2−3°.

Experimental structural results have been reported for compounds **1**−**5**. In Table 1, the energy-optimized structures for these compounds at the MP2 and BPW91 levels are compared with the experimental data. Calculated molecular structures for **6**−**12** are given in the Supporting Information. With few exceptions, the DFT-based bond lengths in Table 1 follow the usual trends[53] in being somewhat longer than those from the MP2 method, and the latter are somewhat larger than the experimental results in the last column. Where experimental errors were given by the authors, they are included in parentheses and apply to the last figure quoted. For aniline and 2-aminopyridine, these are certainly conservative error estimates since the microwave analyses assumed planar rings with $\epsilon = 0°$ (see Figure 1c). In any event, many of the bond lengths and internal angles obtained by both methods are within the experimental errors of the measurements. For aniline, the DFT value for the equilibrium flap angle $\rho_e = 41.4°$ is in fairly good correspondence with a value of about 42° in more detailed analyses.[54,55]

It was of interest to investigate the importance to the magnetic shielding of the large amplitude motions associated with the amine group torsional and tunneling motions. Energy-optimized structures (BPW91/6-311G*) were obtained for aniline (**3**), 2-aminopyrimidine (**8**), and 4-aminopyrimidine (**9**) at 30° intervals of the angles φ and ρ. These molecules present the three situations where the C−NH_2 moiety is flanked by zero, two, and one adjacent nitrogens. The torsion angle φ was taken over a 0−180° range, and the inversion angle ρ varied between −90 and 90°. The 30° grid includes 49 structures, but the symmetry reduced these to 16 structures for aniline and 2-aminopyrimidine and 28 for 4-aminopyrimidine. All geometries are fully optimized at the BPW91/6-311G* level except for the two dihedral angles and the assumption of ring planarity for all structures with $\rho = 0°$.

Depicted in Figure 2a−c for aniline (**3**), 2-aminopyrimidine (**8**), and 4-aminopyrimidine (**9**) are surface plots of the energies ΔE (in millihartrees relative to the lowest energies) as functions of the angles φ and ρ. Also included in the figures are contour plots corresponding to projections of the surface plots on the $\varphi - \rho$ plane. All three plots show very low inversion barriers at $\varphi = 90°$ and $\rho = 0°$ and much higher torsional barriers for $\varphi = 0$ and 180°. In previous studies[56−58] of conformational dependencies of chemical shifts, it was noted that the calculated energies and shift data could be represented accurately by means of Fourier series expansions. In terms of the angle φ and ρ, the energies ΔE are represented by the expression

$$E(\varphi,\rho) = \sum_{n=0,m=0} A_{nm} \cos n\rho \cos m\varphi + B_{nm} \sin n\rho \cos m\varphi \quad (1)$$

where the coefficients A_{nm} and B_{nm} are conveniently determined by multiple linear regression analyses of the calculated data. Each of the energy surfaces for **3**, **8**, and **9**, which are depicted in Figure 2, was analyzed via eq 1, and the coefficients are listed in Table 2.

Of particular interest for aniline in Table 1 are comparisons of the calculated inversion V_i and torsional V_r barriers with the experimental results. Barriers are given in cm^{-1} (1 kcal mol^{-1} corresponds to 349.8 cm^{-1}). The saddle point $V_i = 320$ cm^{-1}

(46) Hehre, W. J.; Ditchfield, R.; Pople, J. A. *J. Chem. Phys.* **1972**, *56*, 2257−2261. Hariharan, P. C.; Pople, J. A. *Theor. Chim. Acta* **1973**, *28*, 213−222.
(47) Møller, C.; Plesset, M. S. *Phys. Rev.* **1934**, *46*, 618−622.
(48) Parr, R. G.; Yang, W. *Density Functional Theory of Atoms and Molecules*; Oxford: New York, 1989. March, N. H. *Electron Density Theory of Atoms and Molecules*; Academic: San Diego, CA, 1992.
(49) Hohenberg, P.; Kohn, W. *Phys. Rev. B* **1964**, *136*, 864−871. Kohn, W.; Sham L. J. *Phys. Rev. A* **1965**, *140*, 1133−1138.
(50) Becke, A. D. *Phys. Rev. A* **1988**, *38*, 3098−3100.
(51) Becke, A. D. *J. Chem. Phys.* **1992**, *96*, 2155−2160. Becke, A. D. *J. Chem. Phys.* **1992**, *97*, 9173−9177. Becke, A. D. *J. Chem. Phys.* **1993**, *98*, 5648−5652.
(52) Wang, Y.; Perdew, J. P. *Phys. Rev. B* **1991**, *44*, 13298−13307. Wang, Y.; Perdew, J. P. *Phys. Rev. B* **1991**, *43*, 8911−8916. Perdew, J. P.; Wang, Y. *Phys. Rev. B* **1992**, *45*, 13244−13249. Perdew, J. P.; Chevary, J. A.; Vosko, S. H.; Jackson, K. A.; Pederson, M. R.; Singh, D. J.; Fiolhais, C. *Phys. Rev. B* **1992**, *46*, 6671−6687.
(53) Andzelm, J.; Wimmer, E. *J. Chem. Phys.* **1992**, *96*, 1280−1303. Johnson, B. G.; Gill, P. M. W.; Pople, J. A. *J. Chem. Phys.* **1993**, *98*, 5612−5626. Neuman, R.; Handy, N. C. *Chem. Phys. Lett.* **1995**, *246*, 381−386. Grabo, T.; Gross, E. K. U. *Chem. Phys. Lett.* **1995**, *240*, 141−150. Edgecombe, K. E.; Becke, A. D. *Chem. Phys. Lett.* **1995**, *244*, 427−432.
(54) Pyka, J.; Kreglewski, M. *J. Mol. Spectrosc.* **1985**, *109*, 207−220. Castellá-Ventura, M.; Kassab, E. *Spectrochim. Acta A* **1994**, *50*, 69−86.
(55) Larson, N. W.; Hansen, E. L.; Nicolaisen, F. M. *Chem. Phys. Lett.* **1976**, *43*, 584−586. Kydd, R. A.; Krueger, P. J. *Chem. Phys. Lett.* **1977**, *49*, 539−543.
(56) Barfield, M.; Yamamura, S. H. *J. Am. Chem. Soc.* **1990**, *112*, 4747−4758. Barfield, M. In *NMR Shielding and Molecular Structure*; Tossell, J. A., Ed.; Kluwer Academic Publishers: Norwell, MA, 1993.
(57) Barfield, M. *J. Am. Chem. Soc.* **1993**, *115*, 6916−6928.
(58) Barfield, M. *J. Am. Chem. Soc.* **1995**, *117*, 2862−2876.

Table 1. Comparison of Calculated Structural Data for **1**−**5** with Experimental Data

compound	bond/angle	MP2/6-311G*	BPW91/6-311G*	expt
benzene[a]	C−C	1.399	1.400	1.3894
	C−H	1.087	1.093	1.0859
pyridine[b]	C1−N2	1.344	1.345	1.3376(4)
	C2−C3	1.398	1.400	1.3938(5)
	C3−C4	1.396	1.398	1.3916(4)
	C2−H	1.088	1.095	1.0857(20)
	C3−H	1.086	1.092	1.0818(18)
	C4−H	1.087	1.092	1.0811(6)
	C2−N1−C6	116.7	116.8	116.94(3)
	N1−C2−C3	123.9	123.9	123.80(3)
	C2−C3−C4	118.7	118.4	118.53(3)
	C3−C4−C5	118.4	118.5	118.40(3)
	N1−C2−H2	115.7	115.7	116.03(9)
	C2−C3−H3	120.1	120.3	120.11(9)
	C3−C4−H4	120.9	120.8	120.80(3)
aniline[c]	C1−C2	1.405	1.411	1.397(3)
	C2−C3	1.396	1.396	1.394(4)
	C3−C4	1.399	1.400	1.396(2)
	C1−N	1.403	1.400	1.402(2)
	C2−H	1.089	1.094	1.082(4)
	C3−H	1.087	1.093	1.083(2)
	C4−H	1.086	1.092	1.080(2)
	N7−H	1.010	1.016	1.001(10)
	C6−C1−C2	118.5	118.3	119.4(2)
	C2−C1−N7	120.6	120.8	120.3(1)
	C1−C2−C3	120.6	120.6	120.1(1)
	C2−C3−C4	120.6	120.8	120.7(1)
	C3−C4−C5	119.1	118.8	118.9(1)
	C3−C2−H2	119.9	119.9	120.1(2)
	C4−C3−H3	120.0	120.0	120.0(1)
	C3−C4−H4	120.5	120.6	120.5(1)
	H−N−H	110.6	111.5	113.1(20)
	ρ_e	46.2	41.4	41.7,[d] 42.17,[e] 46,[f] 42,[g] 37.5 ± 2[c]
	ϵ	3.3	2.8	
	V_i, cm^{-1}	821.2 cm^{-1}	319.9 cm^{-1}	509.0,[d] 524.4,[e] 562,[f] 454 ± 70,[g]
	V_t, cm^{-1}	1555 (ρ = 55.3°)	2200 (55.7°)	1920,[d] 2005 ± 40[e]
pyrimidine[h]	C2−N3	1.341	1.344	1.340(2)
	N3−C4	1.342	1.344	1.340(2)
	C4−C5	1.394	1.397	1.393(2)
	C2−H	1.087	1.094	1.099(7)
	C4−H	1.088	1.095	1.099(7)
	C5−H	1.085	1.091	1.099(7)
	N1−C2−N3	127.6	127.8	127.6(3)
	C2−N3−C4	115.6	115.4	115.5(2)
	N3−C4−C5	122.2	122.5	122.3
	C4−C5−C6	116.8	116.5	116.8
	N3−C4−H	116.3	116.2	115.3(2.8)
2-aminopyridine[i]	N1−C2	1.341	1.349	1.340
	C2−C3	1.409	1.416	1.395
	C3−C4	1.390	1.390	1.394
	C4−C5	1.400	1.403	1.394
	C5−C6	1.393	1.396	1.395
	C6−N1	1.344	1.343	1.340
	C2−N7	1.391	1.386	1.403
	C3−H	1.087	1.093	1.084
	C4−H	1.087	1.093	1.080
	C5−H	1.085	1.091	1.081
	N7−Ha	1.010	1.016	
	N7−Hb	1.008	1.014	
	N1−C2−C3	122.8	122.6	123.9
	C2−C3−C4	118.6	118.4	118.5
	C3−C4−C5	119.0	119.6	118.3
	C4−C5−C6	117.9	117.5	118.5
	C5−C6−N1	124.1	124.4	123.9
	C6−N1−C2	117.5	117.6	116.8
	C3−C2−N7	121.1	121.5	123.9
	C4−C3−H3	121.1	121.0	121.3
	C3−C4−H4	120.1	119.8	120.3
	C4−C5−H5	121.6	121.6	121.3
	N1−C6−H6	115.3	115.2	115.9
	C2−N7−Ha	111.7	113.7	
	C2−N7−Hb	115.0	117.6	
	Ha−N−Hb	113.1	114.7	116.9
	φ_e	82.0	82.8	
	ρ_e	44.0	36.8	30.9

Table 1 (Continued)

compound	bond/angle	MP2/6-311G*	BPW91/6-311G*	expt
	ϵ	3.1	2.3	
	V_i, cm^{-1}	575.4	167.5	

[a] Plíva, J.; Johns, J. W. C.; Goodman, L. *J. Mol. Spectrosc.* **1990**, *140*, 214−225. [b] Sørensen, G. O.; Mohler, L.; Rastrup-Anderson, N. *J. Mol. Struct.* **1974**, *20*, 119−126. [c] Reference 18. [d] Reference 54. [e] Reference 55. [f] Reference 59. [g] Reference 60. [h] Fernholt, L.; Rømming, C. *Acta Chem. Scand. Ser. A* **1978**, *32*, 271−273. [i] Reference 22.

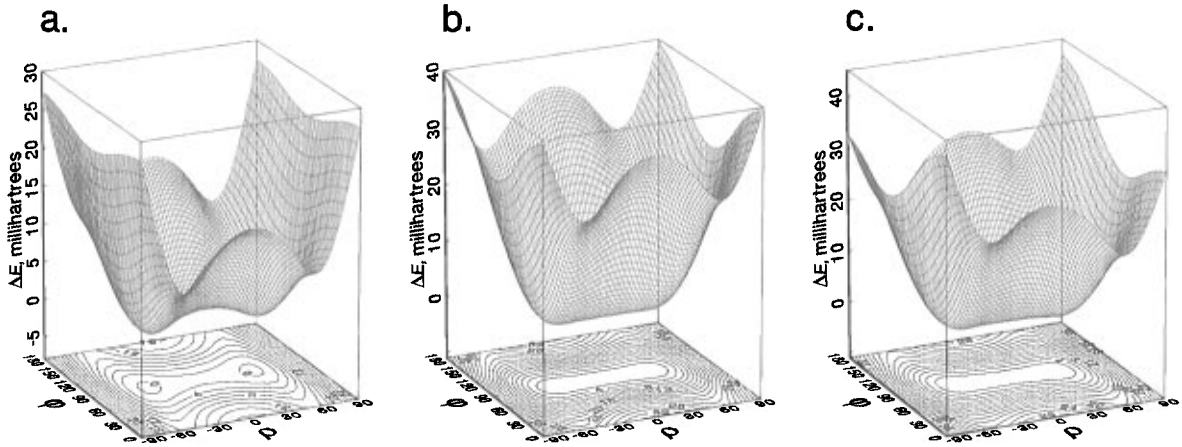

Figure 2. Surface and contour plots of the (BPW91/6-311G*) energies ΔE (in millihartrees relative to the lowest energy, E_0) for **3**, **8**, and **9** as functions of the inversion and torsion angles. The saddle points near (90°, 0°) are the inversion barriers V_i. The torsion barriers V_r are taken as the saddle points along the $\varphi = 0$ and 180° planes. (a) For aniline, $E_0 = -287.625\,202\,3$ hartrees for $\varphi_e = 90°$, $\rho_e = 41.4°$; $V_i = 320$ cm^{-1}, $V_r = 2200$ cm^{-1} at $\rho = 55.7°$. (b) For 2-aminopyrimidine, $E_0 = -319.737\,756\,1$ hartrees for $\varphi_e = 90°$, $\rho_e = 23.7°$; $V_i = 22.7$ cm^{-1}, $V_r = 5558$ cm^{-1} at $\rho = 60.9°$. (c) For 4-aminopyrimidine, $E_0 = -319.734\,666\,9$ hartrees for $\varphi_e = 83.8°$, $\rho_e = 26.0°$; $V_i = 66.3$ cm^{-1}, $V_r = 4010$ cm^{-1} at $\rho = 60.9°$.

at (90°, 0°) in Figure 2a is the calculated (BPW91/6-311G*) inversion barrier. This in an underestimate since the experimental values in Table 1 (which depend on assumptions about the shape of the barrier) range from 424 to 562 cm^{-1}.[54,55,59,60] Also included in Table 1 is the inversion barrier $V_i = 821$ cm^{-1} computed for aniline at the MP2/6-311G* level, which conforms with previous observations that the barrier is substantially overestimated both at the Hartree−Fock and MP2 levels.[23,24] The calculated (BPW91/6-311G*) inversion barriers for 4-aminopyrimidine and 2-aminopyrimidine (66.3 and 22.7 cm^{-1}, respectively) are much smaller than that for aniline. It seems likely that the heights of the inversion barriers are reduced by the decreasing steric hindrance associated with the successive removal of *ortho* hydrogens in this series.

For aniline, the calculated (BPW91/6-311G*) *torsional barrier* of $V_r = 2200$ cm^{-1} ($\varphi = 0$ and $\rho = 55.7°$) in Figure 2a, is much higher in energy than the inversion barriers. It is in fairly good agreement with experimental values in the range of 1920−2005 cm^{-1}, but it is substantially higher than the value of $V_r = 1555$ cm^{-1} computed at the MP2/6-311G* level. The two methods place the angle q to within 0.4°. The torsional barriers increase to 4010 and 5558 cm^{-1} for **9** and **8**, respectively, but $\rho = 60.9°$ in both cases.

The presence of two or more amine groups on an aromatic ring leads to the possibilities of isomers in which each pair of amine groups can be pyramidalized with hydrogens on the same (*syn*) or opposite (*anti*) sides of the ring. The *anti* arrangements have slightly lower calculated energies than *syn*, but the calculated geometries (including the equilibrium inversion angles ρ_e) are quite similar.

B. Shielding Calculations. All magnetic shielding results were based on the GIAO (gauge including atomic orbitals) formulation[28−30] as implemented in the G94 suite of programs.[44] The structures for **1**−**11** were optimized at the MP2/6-311G* and BPW91/6-311G* levels. Because of their similarity to the HF/GIAO results, previous IGLO[31,32] shifts for these molecules are not included here. Shielding calculations were also based on density functional theory (DFT) with BPW91 functionals.[50−52] As implemented in the G94 codes, the DFT functionals do not include a specific magnetic field dependence.[43,44] A recent paper by Cheesemen *et al.*[43] compares the G94 shielding results with a number of functionals including the one adopted here and shows that they are not quite as good as those obtained by Gauss at the MP2 level.[36]

The calculated GIAO ^{13}C, and ^{1}H isotropic magnetic shielding NMR data for CH_4 and the ^{15}N NMR shielding data for NH_3 are entered in Table 3. These are the indirect reference compounds of this study. Molecular structures for CH_4 and NH_3 were optimized at the MP2/6-311G* or BPW91/6-311G* levels as shown in the third column. The shielding calculations were performed at the level indicated in the second column of Table 3. For simplicity in the subsequent discussions and table headings, the abbreviations in the first column describe the level of the calculation. For example, B**M* is a short notation for BPW91/6-311G**//MP2/6-311G*, which implies that the shielding calculation was performed at the BPW91/6-311G* level for a structure optimized at the MP2/6-311G* level.

Chemical shifts were obtained by subtracting the calculated magnetic shielding for the nuclei of interest from the reference compound shielding [tetramethylsilane (TMS) for ^{13}C and ^{1}H, CH_3NO_2 (neat liquid) for ^{15}N]. The ^{13}C shieldings of tetramethylsilane were not obtained explicitly. Rather, the methane shielding data in Table 3 was used in combination with the experimental δ values for gas phase methane (−7.0 and 0.13 ppm for ^{13}C and ^{1}H, respectively).[61−63] For example, the TMS shielding constants at the B**M* level are 184.6 and 31.9 ppm, respectively. Similarly, the ^{15}N reference makes use of the 399.3 ppm difference between liquid CH_3NO_2 and gas phase ammonia.[64,65] All computations were performed using RISC 6000

(59) Brand, J. C. D.; Williams, D. R.; Cook, T. J. *J. Mol. Spectrosc.* **1966**, *20*, 359−380.
(60) Quack, M.; Stockburger, M. *J. Mol. Spectrosc.* **1972**, *43*, 87−116.

Table 2. Coefficients in Eqs 1 and 2 Based on Linear Regression Results for the Calculated BPW91/6-311G* Energies and BPW91/6-311G* Isotropic Shielding Data for Some Nuclei of Aniline and 2-Aminopyrimidine[a]

compound	A_{00}	A_{10}	A_{20}	A_{30}	A_{02}	A_{12}	A_{22}	A_{32}	A_{04}	A_{14}	A_{24}	A_{34}	A_{06}	A_{16}	A_{26}	A_{36}	SD
								Aniline									
ΔE	61.6	−84.1	35.6	−4.3	2.7	3.7	1.2	0.0	2.2	−3.3	2.2	−0.7	0.7	−1.2	0.7	−0.3	0.07
C1	159.6	−14.1	0.3	0.8	−1.0	0.9	0.3	0.1	1.4	−2.3	1.4	−0.5	0.1	−0.2	0.2	0.0	0.08
C4	122.7	1.8	−2.7	0.5	3.4	1.1	1.5	−0.2	1.6	−2.4	1.6	−0.5	0.7	−1.0	0.7	−0.2	0.09
N	−317.5	−20.7	0.6	−4.3	−10.6	−6.7	−2.3	−0.7	−20.3	33.7	−19.3	6.4	−8.2	13.5	−8.2	2.7	0.07
								2-Aminopyrimidine									
ΔE	62.2	−71.9	29.1	−2.7	9.7	4.2	3.6	−0.4	7.9	−12.5	7.7	−2.6	2.0	−3.2	2.0	−0.7	0.05
C2	179.6	−14.5	−1.3	1.2	0.0	1.6	0.4	0.0	2.6	−4.0	2.4	−0.8	0.9	−1.4	0.9	−0.3	0.09
C5	115.5	3.1	−3.1	0.8	2.2	1.6	0.4	0.1	2.1	−3.2	2.1	−0.7	0.8	−1.3	0.8	−0.3	0.06
N7	−265.5	−70.9	25.2	−9.1	−13.2	−6.5	−4.4	0.0	−31.4	50.9	−30.8	10.2	−7.5	12.1	−7.6	2.5	0.10

Coefficients in Eqs 1 and 2 Based on Linear Regression Results for the Calculated BPW91/6-311G* Energies and BPW91/6-311G* Isotropic Shielding Data for some Nuclei of Aniline, 2-Aminopyrimidine, and 4-Aminopyrimidine[a]

compound	A_{00}	A_{10}	A_{20}	A_{30}	B_{11}	B_{21}	B_{31}	A_{02}	A_{12}	A_{22}	A_{32}	A_{04}	A_{14}	A_{24}	A_{34}	SD
								Aniline								
C2,C6[b]	121.6	5.4	−3.5	1.0	−2.6	1.5	−0.3	7.2	3.5	3.5	−0.4	4.7	−7.3	4.8	−1.5	0.15
C3,C5[c]	132.0	−2.4	1.1	−0.3	−1.0	0.5	−0.1	0.1	−0.4	0.2	0.0					0.05
								2-Aminopyrimidine								
C4,C6[d]	160.0	0.1	−0.1	0.1	−0.9	0.5	−0.2	0.8	0.0	0.5	−0.1					0.12
N1,N3[e]	−99.3	29.6	−18.0	5.5	−7.1	4.7	−0.9	20.4	6.2	8.8	−1.4	20.9	−32.1	21.2	−6.7	0.51
								4-Aminopyrimidine								
ΔE[f]	63.4	−76.9	30.9	−3.1	−5.4	1.5	−0.2	7.7	4.3	2.9	−0.4	6.4	−10.0	6.3	−2.2	0.13
C2[g]	161.5	3.0	−1.5	0.5	−1.4	0.8	−0.2	0.7	0.3	0.3	0.0					0.12
C4[h]	175.4	−11.5	−3.0	1.8	0.2	−0.6	0.2	0.7	2.2	0.5	0.1	4.5	−6.9	4.2	−1.4	0.13
C5[i]	108.0	12.8	−7.9	2.7	1.7	−1.2	0.5	5.9	5.4	1.8	0.0	10.4	−16.2	10.4	−3.5	0.21
C6[j]	161.1	−3.0	1.3	−0.5	0.7	−0.3	0.0	0.7	0.5	0.3	0.0					0.10
N1[k]	−79.5	7.6	−7.5	1.6	0.7	0.0	0.0	9.3	3.4	3.5	−0.5	4.8	−6.6	4.5	−1.5	0.24
N3[l]	−90.8	16.5	−11.3	3.4	−8.1	4.0	−0.9	19.8	6.0	9.1	−1.5	12.0	−17.4	12.6	−3.8	0.35
N7[m]	−285.0	−49.3	14.3	−6.2	4.3	−3.6	1.0	−16.2	−1.9	−7.3	0.8	−23.9	38.5	−23.3	7.6	0.45

[a] The coefficients are defined in eq 1. Other nonzero coefficients are given below. All energies are in millihartrees and chemical shifts are in ppm. Standard deviations (SD) of the linear regressions are given in the last column. [b] $B_{13} = 0.2$, $B_{23} = -0.1$, $B_{33} = -0.1$. [c] $B_{13} = -0.1$. [d] $B_{13} = -0.2$, $B_{23} = -0.1$. [e] $B_{13} = 1.6$, $B_{23} = -1.7$, $B_{33} = 0.5$. [f] $B_{13} = 0.6$, $B_{23} = -0.7$, $B_{33} = 0.1$. [g] $B_{13} = -0.2$. [h] $B_{13} = 0.4$. [i] $B_{13} = -0.2$, $B_{23} = -0.1$, $B_{33} = -0.1$. [j] $B_{13} = 0.6$, $B_{23} = -0.1$, $B_{33} = 0.1$. [k] $B_{13} = 0.2$, $B_{23} = -0.2$. [l] $B_{13} = 1.4$, $B_{23} = -1.3$, $B_{33} = 0.2$. [m] $B_{13} = -0.9$, $B_{23} = 0.7$.

Table 3. Calculated GIAO ^{1}H, ^{13}C, and ^{15}N Magnetic Shieldings in ppm for the Reference Compounds CH_4 and NH_3 Using Several HF and DFT Methods[a]

notation	shielding	structure	$\sigma(^1\mathrm{H})$	$\sigma(^{13}\mathrm{C})$	$\sigma(^{15}\mathrm{N})$
H*M*	HF/6-311G*	MP2/6-311G*	32.10 (32.04)	195.9 (195.6)	271.9 (269.6)
H**M*	HF/6-311G**	MP2/6-311G*	31.78 (31.72)	196.5 (196.2)	274.0 (271.7)
B**M*	BPW91/6-311G**	MP2/6-311G*	31.81 (31.75)	191.6 (191.2)	272.3 (269.6)
B*B*	BPW91/6-311G*	BPW91/6-311G*	31.81 (31.72)	189.5 (188.8)	266.2 (264.5)
B**B*	BPW91/6-311G**	BPW91/6-311G*	31.54 (31.45)	189.7 (189.0)	267.6 (265.9)

[a] All values in ppm. Isotropic shielding data in parentheses arise for the cases in which the reference molecules were optimized at the corresponding 6-31G* level.

IBM590 workstations. The 3D surface plots and contour plots were generated by a commercial plotting package which includes 2D and 3D spline algorithms (cubic or bicubic spline interpolation).[66]

For aniline, 2-aminopyrimidine, and 4-aminopyrimidine it was convenient to analyze chemical shift data in terms of truncated Fourier series analogous to eq 1 (eq 2). Entered in Table 2 are

$$\delta(\varphi,\rho) = \sum_{n=0,m=0} A_{nm} \cos n\rho \cos m\varphi + B_{nm} \sin n\rho \cos m\varphi \tag{2}$$

the coefficients A_{nm} and B_{nm} which occur in the expressions for the ^{13}C and ^{15}N shifts of the three molecules. The conformationally averaged chemical shifts $\langle\delta_i\rangle$ are calculated as the weighted average of the $\delta_i(\varphi,\rho)$ surfaces with respect to the energy surfaces $E_i(\varphi,\rho)$. The averaged chemical shifts $\langle\delta_i\rangle$ were obtained by numerical integration of eq 3.

$$\langle\delta_i\rangle = \int \delta_i(\varphi,\rho)\, e^{-Ei(\varphi,\rho)/kT}\, \mathrm{d}\varphi\, \mathrm{d}\rho / \int e^{-Ei(\varphi,\rho)/kT}\, \mathrm{d}\varphi\, \mathrm{d}\rho \tag{3}$$

As noted previously, diamino compounds having the NH_2 groups pyramidalized *anti* have slightly lower energies than the *syn* isomers. Compounds **7**, **11**, and **12** have three NH_2 groups. The number of isomers increases (2, 3, and 4, respectively) with decreasing symmetry. In some cases this leads to a nonequiva-

(61) Previous reports of isotropic ^{13}C NMR chemical shifts from these laboratories[56−58] used an early criterion from the Bochum group[31,32] with −2.3 ppm for the methane reference. With this value, for example, the average deviation between calculated (IGLO, with a triple-ζ basis set) and experimental ^{13}C NMR shifts for 16 carbons in a series of 1-substituted butanes was +2.2 ppm.[58] On the basis of the −7.0 ppm value for gas phase methane, the average deviation for the same set of data is −2.5 ppm.

(62) Jameson, A. K.; Jameson, C. J. *Chem. Phys. Lett.* **1987**, *134*, 461−466.

(63) Emsley, J. W.; Feeney, J.; Sutcliffe, L. H. *High Resolution Nuclear Magnetic Resonance*; Pergamon: Oxford, U.K., 1966; Vol. 2. The experimental gas phase data were converted as described by Kutzelnigg *et al.*[32]

(64) Mason, J. In *Multinuclear NMR*; Mason, J., Ed.; Plenum: New York, 1987; pp 335−367. Litchman, W. M.; Alei, M., Jr.; Florin, A. E. *J. Chem. Phys.* **1969**, *50*, 1031−1032. Alei, M., Jr.; Florin, A. E.; Litchman, W. M.; O'Brien, J. F. *J. Phys. Chem.* **1971**, *75*, 932−938.

(65) A similar value, 400.9 ppm, was suggested: Witanowski, M.; Stefaniak, L.; Webb, G. A. *Annu. Rep. NMR Spectrosc.* **1993**, *25*, 88.

(66) Axum: Technical Graphics and Data Analysis, 2nd ed.; TriMatrix, Inc.: Seattle, WA, 1992.

Table 4. Comparisons of Calculated GIAO ^{13}C NMR Shifts with Experimental Data for a Series of Aminopyrimidines and Aminobenzenes[a]

cmpd	atoms	H*M*	H**M*	B**M*	B*B*	B**B* [b]	expt[c]
1[d,e]	C1-C6	130.0	131.7	131.7	129.1	130.3	128.40 (130.9)
2[f,g]	C2,C6	155.3	157.1	154.5	151.7	153.1	150.6 (149.10)
	C3,C5	120.6	122.1	126.3	124.0	125.1	124.5 (122.85)
	C4	140.7	142.3	137.0	134.9	136.0	136.4 (134.80)
3[h,i]	C1	152.9	153.8	150.6	148.7	149.1 (−0.6)	148.7 (146.90)
	C2,C6	113.2	114.8	116.4	113.2	114.5 (−0.3)	114.4 (115.41)
	C3,C5	134.2	135.9	132.1	129.5	129.7 (0.0)	129.1 (129.41)
	C4	117.5	119.1	121.0	118.0	119.1 (−0.4)	116.3 (118.59)
4[j,k]	C2	166.4	168.3	165.8	162.8	164.3	159.6 (158.39)
	C4,C6	163.6	165.3	159.9	157.5	158.8	157.1 (156.90)
	C5	114.5	116.0	123.9	122.3	123.3	121.8 (121.86)
5[h,l]	C2	166.7	166.8	161.1	159.0	159.3	161.4 (160.4)
	C3	103.3	104.8	109.6	106.3	107.4	109.7 (109.5)
	C4	145.6	147.3	138.5	136.2	137.4	138.6 (138.1)
	C5	109.3	110.8	116.8	113.8	114.9	113.6 (114.0)
	C6	156.0	157.8	152.6	149.9	151.2	149.2 (149.0)
6[m−o]	C1,C3	156.0	157.0	151.1	149.4	149.8	147.9 (147.74)
	C2	97.5	99.0	101.2	97.5	99.0	102.2 (105.66)
	C4,C6	102.0	102.9	107.0	103.8	105.1	106.2 (106.06)
	C5	138.1	139.3	132.3	129.6	130.8	130.4 (130.32)
7[p]	C1,C3	158.8	159.8	151.3	149.6	150.0	
	C2	87.1	88.6	92.8	89.6	90.9	
	C4,C6	87.2	88.7	92.9	89.7	91.1	
	C5	158.9	159.7	151.4	149.7	150.1	
8[q,r]	C2	170.3	170.9	166.2	164.0	164.3 (−0.1)	163.54 (163.42)
	C4,C6	166.8	168.6	160.2	157.9	159.1 (0.0)	157.96 (157.85)
	C5	103.7	105.2	114.6	111.7	112.8 (0.0)	110.06 (110.04)
9[q,r]	C2	166.9	168.8	163.3	161.0	162.4 (0.0)	158.32 (158.27)
	C4	171.0	171.7	163.0	160.7	161.0 (−0.2)	163.22 (163.19)
	C5	97.2	98.6	106.7	103.3	104.4 (−0.3)	104.99 (105.06)
	C6	165.2	167.0	158.9	156.5	157.9 (0.0)	154.70 (154.62)
10[m,r]	C2	167.9	169.7	161.7	159.4	160.7	157.7
	C4,C6	172.7	173.4	164.0	162.2	162.5	163.3
	C5	77.0	78.4	85.4	81.8	82.9	82.6
11[q−s]	C2	171.0	171.5	164.0	162.9	163.0	163.07 (162.8)
	C4	174.3	175.0	164.5	163.1	163.4	164.50 (164.3)
	C5	69.1	70.5	78.1	75.3	76.5	74.82 (74.8)
	C6	174.3	175.0	164.6	163.3	163.5	164.50 (164.3)
12[q,t]	C2	171.3	171.9	164.5	163.0	163.2	163.48[u]
	C4	174.9	175.6	165.1	164.3	164.5	165.16[u]
	C5	68.8	70.0	77.6	73.6	74.5	73.74
	C6	174.8	175.5	163.4	161.6	161.7	162.73[u]
av dev.		6.6	7.0	2.2	1.3	1.5	
rms dev.		7.1	7.7	2.7	1.7	1.9	

[a] All values in ppm relative to TMS. The ^{13}C shieldings for TMS were based on the calculated values for CH_4 in Table 1 and the experimental gas phase value δ −7.0 for CH_4. The solvent is DMSO-d_6 unless noted otherwise. [b] Differences between values computed with chemical shifts averaged with respect to torsional and inversion motions $\langle\delta_i\rangle$ and those obtained for the minimum energy conformation δ_i are given in parentheses. [c] References to the experimental chemical shifts are given in the first column. [d] Benzene, neat: Breitmaier, E.; Hass, G.; Voelter, W. *Atlas of Carbon-13 NMR Data*; Plenum: New York, 1976. [e] Benzene gas phase. Reference 62. [f] Reference 2. [g] Pyridine, neat: Breitmair, Haas and Voelter, footnote d. [h] Formácek, V.; Desnoyer, L.; Kellerhals, H. P.; Keller, T.; Clerc, J. T. ^{13}*C Data Bank*; Bruker Physik: Karlsruhe, 1976; Vol 1. [i] Reference 10. [j] Measured in benzene-d_6: Formácek *et al*., footnote h. [k] Reference 12. [l] Measured in CCl_4.[14] [m] Calculated data for the species with slightly lower energy having one of the NH_2 groups puckered in the opposite direction. [n] Chloroform-*d* solvent: Formácek *et al*., footnote h. [o] Reference 10. [p] The calculated values all apply to the isomer which has one of the NH_2 groups puckered in the opposite sense to the other two, as this has a slightly lower energy. The decrease in symmetry makes the carbons nonequivalent, but these are not listed separately since the differences are less than 0.1 ppm. [q] This work. [r] Reference 15. [s] Calculated results are for the isomer which has one of the NH_2 groups at C4 or C6 puckered in the opposite sense to the NH_2 at C2 ($2^+4^-6^+$). [t] Data are for the lowest energy isomer ($2^+4^-6^+$). Geometry optimizations for **12** were carried out at the MP2/6-31G* and BPW91/6-31G* levels. [u] These values may be interchanged. This ordering was chosen to make the values consistent with those calculated via B**M*, B*B* and B**B*.

lence in the calculated chemical shifts which would not ordinarily be observable because of rapid interconversion. The calculated results in Table 4−6 are those for the lowest energy (*anti*) isomers. For compounds **11** and **12**, the lowest energy isomers are designated $2^+4^-6^+$ to indicate that the NH_2 groups at C2 and C6 are puckered in a sense opposite to the NH_2 group at C4. The computed ^{13}C NMR chemical shifts for the various isomers differ by 0.3 ppm at most. Differences in the ^{15}N NMR chemical shifts are larger, varying by as much as 0.8 ppm for the aromatic nitrogens in **11** and **12**. On average, the ring nitrogens associated with the *anti* arrangements of the amine groups are 0.6 ppm more shielded than those for the *syn* arrangements.

III. Experimental Section

All compounds except **12** were obtained from Aldrich Chemical Company and were used without further purification. Desoxyminoxidil was obtained from the Upjohn Company Fine Chemical division. Each NMR sample (^{1}H, ^{13}C, and ^{15}N) was 0.2 M using DMSO-d_6 (ISOTEC) as solvent.

The ^{1}H and ^{13}C NMR spectra were obtained on a Bruker Instruments AMX-400 spectrometer at 400.13 and 100.62 MHz, respectively, using 5 mm o.d.tubes (Wilmad). The ^{15}N NMR spectra were obtained with a Bruker Instruments AMX-500 spectrometer at 50.68 MHz using 10 mm o.d. tubes (Wilmad). Decoupled ^{13}C and ^{15}N NMR spectra were obtained using a WALTZ-16 pulsed decoupling scheme[67] with a 99 μs 180° flip angle.

Table 5. Comparisons of Calculated GIAO ^{15}N NMR Shifts with Experimental Data for a Series of Aminopyrimidines and Aminobenzenes[a]

cmpd	atoms	H*M*	H**M*	B**M*	B*B*	B**B* [b]	expt[c]
2[d,e]	N1	−20.5	−16.7	−30.3	−37.9	−35.0	−63.1 (−54.6)
3[f]	N7	−337.3	−335.8	−312.4	−316.6	−315.4 (−2.4)	−320.0 (−318.8)[i]
4[g,h]	N1,N3	−61.0	−57.5	−53.0	−61.0	−58.4	−83.90 (−84.8)
5[h]	N1	−84.1	−80.6	−84.0	−92.7	−89.8	−113.8
	N7	−324.9	−323.3	−300.1	−304.6	−303.2	−307.3 (−304.6)[i]
6[i,j]	N7,N8	−335.8	−334.3	−313.1	−317.2	−316.0	−319.1
7[j]	N7,N8	−333.8	−332.3	−313.0	−317.9	−316.7	
		N9	−333.7	−332.2	−312.8	−317.8	−316.6
8[h,k]	N1,N3	−120.1	−116.7	−105.3	−114.0	−111.3 (−0.2)	−129.9
	N7	−317.2	−315.3	−292.6	−297.6	−296.0 (0.0)	−297.9
9[k]	N1	−99.2	−95.6	−84.5	−93.2	−90.3 (−0.6)	−122.3[l]
	N3	−117.7	−114.4	−104.3	−112.6	−110.0 (−0.3)	−132.0[l]
	N7	−321.0	−319.2	−297.6	−302.3	−300.7 (−0.6)	−297.2
10[k,j]	N1,N3	−139.9	−136.5	−122.6	−130.8	−127.9	−149.4
	N7,N8	−321.1	−319.3	−299.8	−304.2	−302.8	−309.1
11[k,m]	N1	−184.1	−180.9	−166.0	−172.7	−170.0	−189.5
	N3	−184.2	−181.0	−166.2	−172.9	−170.2	−189.5
	N7	−316.5	−314.7	−297.3	−301.9	−300.6	−304.0
	N8,N9	−320.5	−318.7	−301.4	−305.9	−304.5	−306.0
12[k,n]	N1	−186.2	−183.5	−169.0	−177.7	−175.6	−188.5
	N3	−186.1	−183.0	−169.9	−173.4	−170.8	−189.8
	N7	−317.9	−316.1	−298.8	−302.6	−301.3	−303.3
	N8	−321.7	−319.9	−302.7	−306.2	−304.9	−305.9
	N9	−309.1	−306.9	−273.1	−276.9	−275.4	−296.5
av dev.		15.7	16.5	17.0	11.5	13.4	
rms dev.		18.1	19.0	20.5	14.8	16.8	

[a] All values in ppm relative to neat CH_3NO_2. The CH_3NO_2 shielding values were based on the calculated values for NH_3 in Table 1 and the experimentally determined value −399.3 ppm. The solvent is DMSO-d_6 unless noted otherwise. [b] Differences between values computed with chemical shifts averaged with respect to torsional and inversion motions $\langle\delta_i\rangle$ and those obtained for the minimum energy conformation δ_i are given in parentheses. [c] References to experimental chemical shifts are given in the first column. [d] Reference 65, p 282. [e] Gas phase.[65] [f] Reference 65, p 128. [g] Reference 65, p 291. [h] Reference 17. [i] Reference 11. [j] Lowest energy isomer with the amine groups puckered in opposite senses. [k] This work. [l] These values may be interchanged. This order was chosen to be consistent with the calculated data. [m] One of the NH_2 groups at C4 or C6 is puckered in the opposite sense to the NH_2 at C2 ($2^+4^-6^+$). [n] Results obtained for the $2^+4^-6^+$ isomer. Geometry optimizations for **12** were carried out at the MP2/6-31G* and BPW91/6-31G* levels.

All spectra were recorded at 300 K with 20 Hz sample spinning. The ^{1}H NMR spectra used 10.96 ppm spectral widths collected into 4K complex data points with zero-filling to 8K points. Four scans were coadded. The chemical shifts were referenced to the residual protiosolvent at δ 2.490. The ^{13}C NMR data were obtained with the following: spectral widths of 22 727 Hz collected into 32K complex points; a 45° pulse angle and 2 s recycle delay; time averaging of 4096 scans. Chemical shifts were referenced to the solvent multiplet at δ 39.5. The ^{15}N NMR data were obtained with the following: spectral widths of 365.34 ppm collected into 32K complex points; a 30° pulse angle and 2 s recycle delay; time averaging of 20 000 scans. All ^{15}N NMR chemical shifts were referenced by first obtaining the ^{1}H-decoupled NMR spectrum of $^{15}NH_4Cl$ (99% ^{15}N), referencing the single peak at δ −352.0 relative to CH_3NO_2 and then changing samples. The chemical shift data are collected in Tables 4−6 along with values from the literature.

IV. Comparisons of Calculated Chemical Shifts with Experimental Values

A. Carbon Shifts. Entered in Table 4 are the calculated and experimental isotropic ^{13}C NMR chemical shifts (δ_i) for **1**−**12**. Calculated GIAO results at the SCF level with MP2-based geometries (H*M* and H**M*) are given in the third and fourth columns. For pyridine (**2**) and pyrimidine (**4**), the GIAO/SCF values are quite similar to the IGLO results reported by Schindler.[8] In the next three columns of Table 4 are the DFT/GIAO chemical shift obtained with MP2 (B**M*) and DFT (B*B* and B**B*) optimized structures. The average deviations and the root-mean-square deviations between calculated and experimental shifts are given at the bottom of columns.

The calculated GIAO/DFT isotropic ^{13}C NMR chemical shifts from Table 4 are plotted in Figure 3 versus the experimental data for all (37) aromatic carbons (not including those of 1,3,5-triaminobenzene) for which experimental data are available. Because the ^{13}C NMR chemical shifts are poorly reproduced at the Hartree−Fock (HF) level, only the GIAO/DFT results are included in Figure 3. It can be seen that the calculated results at the B**M*, B*B*, and B**B* levels (as represented by open circles, squares, and triangles, respectively) are comparable. There is excellent agreement with the experimental data since the solid line in Figure 3 has unit slope and zero intercept. Even though all of the carbons are aromatic, the range of nearly 100

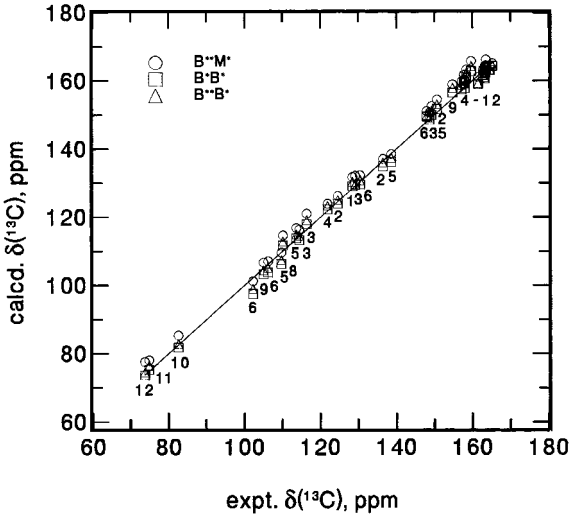

Figure 3. The calculated isotropic ^{13}C NMR chemical shifts are plotted versus the experimental data for all carbons of **1**−**6** and **8**−**12**. The following DFT results from Table 4 are included: B**M* level (○), the B*B* level (□), and the B**B* level (△). The solid line has unit slope and zero intercept.

(67) Shaka, A. J.; Keeler, J.; Freeman, R. *J. Magn. Reson.* **1983**, *53*, 313−340.

Table 6. Comparisons of Calculated GIAO ^{1}H NMR Shifts with Experimental Data for a Series of Aminopyrimidines and Aminobenzenes[a]

cmpd	atoms	H*M*	H**M*	B**M*	B*B*	B**B*	expt[b]
1[c]	H1-H6	7.37	7.43	7.66	7.29	7.47	7.27
2[d]	H2,H6	8.81	8.82	9.08	8.73	8.89	8.52
	H3,H5	7.00	7.09	7.40	7.04	7.24	7.16
	H4	7.79	7.85	7.83	7.44	7.64	7.55
3[e]	H2,H6	6.50	6.61	6.76	6.33	6.55	6.52
	H3,H5	7.32	7.36	7.36	6.99	7.15	7.03
	H4	6.61	6.68	6.91	6.52	6.69	6.64
4[f]	H2	9.35	9.33	9.79	9.44	9.57	9.26
	H4,H6	8.91	8.91	9.06	8.70	8.87	8.87
	H5	6.72	6.87	7.25	6.87	7.13	7.58
5[g]	H3	6.11	6.23	6.53	6.09	6.31	6.70
	H4	7.69	7.73	7.51	7.10	7.28	7.44
	H5	6.27	6.38	6.70	6.29	6.50	6.60
	H6	8.38	8.37	8.43	8.08	8.23	8.11
6	H2	5.66	5.83	5.92	5.42	5.68	
	H4,H6	5.79	5.91	6.10	5.66	5.88	
	H5	7.21	7.23	7.04	6.67	6.82	
7	H2,H4, H6	5.00	5.17	5.32	4.85	5.11	
8[h,i]	H4,H6	8.55	8.52	8.48	8.12	8.27	8.19 (8.15)
	H5	5.97	6.14	6.50	6.03	6.30	6.52 (6.49)
9[h,i]	H2	8.76	8.72	8.98	8.66	8.78	8.31 (8.40)
	H5	5.81	5.98	6.36	5.88	6.15	6.39 (6.27)
	H6	8.51	8.50	8.49	8.12	8.27	8.01 (8.10)
10[h,j]	H2	8.34	8.28	8.39	8.09	8.21	8.01
	H5	4.88	5.07	5.44	4.94	5.22	5.49
11[h]	H5	4.37	4.58	4.96	4.48	4.77	4.83
12[h]	H5	4.46	4.68	5.16	4.53	4.85	4.70
av dev.		0.33	0.28	0.28	0.25	0.19	
rms dev.		0.39	0.32	0.33	0.32	0.23	

[a] All values in ppm relative to TMS. The TMS shieldings were based on the calculated values for CH_4 and the experimentally determined gas phase value δ 0.13. The solvent is DMSO-d_6 unless noted otherwise. The amine group orientations for **6**, **7**, **10**, **11**, and **12** correspond to the lowest energy arrangements as described in the text and the footnotes to Tables 4 and 5. [b] References to the experimental chemical shifts are given in the first column. [c] Reference 59. [d] CCl_4 solvent.[5] [e] C_6H_6 solvent.[1] [f] Gronowitz, S.; Hoffman, R. A. *Ark. Kemi* **1960**, *16*, 459−469. Reddy, G. S.; Hobgood, R. T., Jr.; Goldstein, J. H. *J. Am. Chem. Soc.* **1962**, *84*, 336−340. [g] Brugel, W. *Z. Electrochem.* **1962**, *66*, 159−177. [h] This work. [i] Measured in CCl_4.[15] [j] These values are for the hemisulfate salt.

ppm is about half of the total ^{13}C NMR chemical shift range. Linear regression analyses for the three DFT data sets yield the following results all having $r^2 = 0.996$ and standard deviation 1.8 ± 0.1 ppm.

$$\delta(\text{B**M*}) = 0.996\delta_{\text{exp}} + 3.67 \text{ ppm} \quad (4a)$$

$$\delta(\text{B*B*}) = 1.010\delta_{\text{exp}} - 1.65 \text{ ppm} \quad (4b)$$

$$\delta(\text{B**B*}) = 1.002\delta_{\text{exp}} + 0.28 \text{ ppm} \quad (4c)$$

Results at the B**B* level in eq 4c have the closest slope to unity and the smallest intercept. The prediction of chemical shifts to this accuracy is remarkable, considering that solvent effects were not considered and most shifts were measured in DMSO.

In Figure 3 it can be seen that the aromatic carbons at highest frequency are those in the range of 150−167 ppm for the *ipso* and *meta* (C2, C4, and C6) carbons of the aminopyrimidines. Since the numbering of the ring system relative to the position of an NH_2 group differs for the various compounds, it is convenient to identify the positions as *ipso*, *ortho*, *meta*, and *para*. Progressive amine substitutions produce the largest variations of 73−130 ppm at the *para* (C5) carbon. In section V it will be shown that these trends parallel the electron population changes with progressive amine substitutions.

The data in Table 4 clearly show that the inclusion of hydrogen polarization functions slightly increases the GIAO calculated ^{13}C NMR shifts. Calculated HF and DFT results for all carbons are greater by averages of 1.3 and 0.9 ppm, respectively, if polarization functions are included. There are also clear trends in the calculated ^{13}C NMR chemical shifts depending on whether the geometries are optimized at the MP2 or DFT levels. All of the ^{13}C NMR chemical shifts in Table 4 (B**B* in column 7) for molecules with DFT-optimized geometries are less (by an average 1.6 ppm) than those obtained with MP2-optimized structures (B**M* in column 5), reflecting the consistent geometrical differences in Table 1.

Differences between the H**M* and B**M* data in Table 4 indicate the importance of including electron correlation in the GIAO calculations. These differences reflect several interesting trends. *Electron correlation effects increase monotonically with the number of NH_2 substituents.* Differences between the GIAO/DFT and GIAO/SCF schemes are smallest (<0.1 ppm) for benzene and greatest (ca. −12 ppm) for the C6 carbon of **12**, e.g., the last entry in Table 4. In all cases, GIAO/SCF calculations *underestimate* the ^{13}C NMR chemical shifts at *ortho* and *para* carbons and *overestimate* the shifts for *ipso* and *meta* carbons. Electron correlation effects implicit in GIAO/DFT reduce the differences between the shifts of the two sets and bring them into conformity with the experimental data. This parallels the changes which occur in the electron densities on introducing electron correlation effects.[68] In section V, it will be shown that NH_2 substitution leads to Mulliken $2p_z$ populations[69] (at the DFT/STO-3G level) which are more positive than HF/STO-3G values for *ortho* and *para* atoms and more negative values for atoms at *ipso* and *meta* ring positions.

Also included in Table 4 for aniline, 2-aminopyrimidine, and 4-aminopyrimidines are results which reflect the importance of conformational averaging to the calculated ^{13}C NMR shifts. Chemical shifts were computed by numerical integration (ac-

(68) Carpenter, J. E.; McGrath, M. P.; Hehre, W. J. *J. Am. Chem. Soc.* **1989**, *111*, 6154−6156.
(69) Mulliken, R. S. *J. Chem. Phys.* **1955**, *23*, 1833−1840.

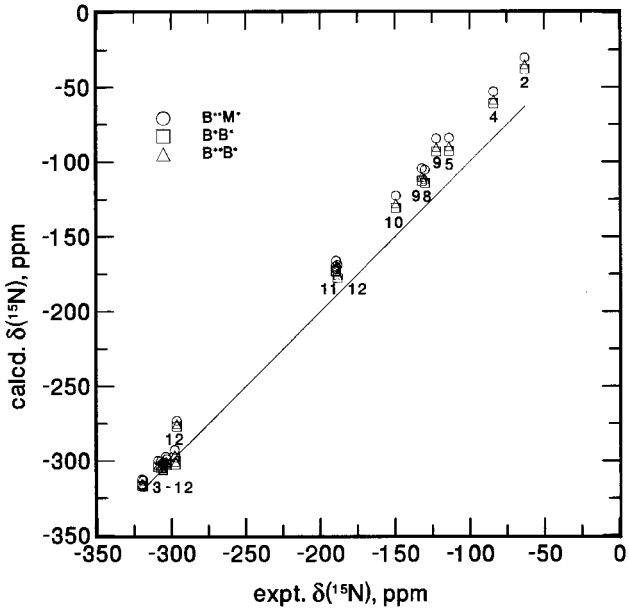

Figure 4. The calculated ^{15}N NMR chemical shifts are plotted versus the experimental data for **2**−**12** (except **7**). The following calculated results obtained are indicated: B**M* (○), B*B* (□), and B**B* (△) levels. The solid line has unit slope and zero intercept.

cording to eq 3) of the calculated shifts $\delta(\mathrm{C}i,\varphi,\rho)$ with respect to the energy contours $\Delta E(\varphi,\rho)$ depicted in Figures 2a−c. Differences in Table 4 between the averaged results $\langle\delta_i\rangle$ and those obtained at the minimum energy conformation δ_i are given in parentheses in the next to last column. Since the largest change is only −0.6 ppm (for the C1 carbon of aniline), it appears that conformational averaging is not an important consideration for the (small) disparities between the calculated and experimental ^{13}C NMR data.

B. Nitrogen Chemical Shifts. Entered in Table 5 are the calculated and experimental isotropic ^{15}N NMR chemical shifts $\delta_i(^{15}\mathrm{N})$ for **2**−**12**. The calculated GIAO/DFT shifts are plotted in Figure 4 versus the available experimental ^{15}N NMR chemical shifts for all (21) aromatic and NH_2 nitrogens. Calculated results at the B**M*, B*B*, and B**B* levels are comparable. Linear regression yields the following (in all cases $r^2 = 0.998$ and the standard deviations are 5.15 ± 0.15 ppm):

$$\delta(\mathrm{B{**}M{*}}) = 1.129\delta_{\mathrm{exp}} + 43.4\ \mathrm{ppm}$$

$$\delta(\mathrm{B{*}B{*}}) = 1.098\delta_{\mathrm{exp}} + 32.8\ \mathrm{ppm}$$

$$\delta(\mathrm{B{**}B{*}}) = 1.105\delta_{\mathrm{exp}} + 36.2\ \mathrm{ppm}$$

Since the solid line in Figure 4 corresponds to the line of unit slope and zero intercept, ^{15}N NMR chemical shifts of the aromatic nitrogens are not predicted as well as for amine nitrogens or for the ^{13}C NMR shifts of aromatic carbons in Figure 3.

The chemical shifts for NH_2 nitrogens in Figure 4 cluster in a 60 ppm range, while the aromatic nitrogens cover a larger range of about 150 ppm. This suggests that the calculated results could remove certain ambiguities in the experimental data. For example, the ring nitrogen shifts of 4-aminopyrimidine (**9**) at −122 and −132 ppm in Table 5 were assumed to conform to the calculated results, all of which have more positive values for N1 than for N3. The computed ^{15}N NMR chemical shifts follow all of the trends noted previously for ^{13}C shifts, but the NH_2 nitrogens fall into different ranges than the aromatic nitrogens. For example, polarization functions on hydrogens lead to larger shifts for all nitrogens, but the average increases at the GIAO/SCF level are 3.3 ppm for aromatic nitrogens and 1.8 ppm for NH_2 nitrogens. At the GIAO/DFT level, the average chemical shift changes on including hydrogen polarization functions are 2.7 and 1.4 ppm, respectively. These are consistent trends since the standard deviations in all cases are less than 10% of the averages. Furthermore, all ^{15}N NMR shifts computed (B**B*) with DFT-optimized geometries are smaller than those computed (B**M*) with MP2-optimized geometries by averages of 5.0 and 3.0 ppm for aromatic and NH_2 nitrogens, respectively. The importance to ^{15}N NMR shifts of including the electron correlation effects, which are implicit in the DFT methods, is indicated by subtracting the calculated H**M* values from the B**M* values in Table 5. These differences range from −14 ppm for pyridine to +34 ppm for the piperidine nitrogen (N6) of **12**. For the NH_2 groups correlation effects increase the calculated shifts by an average of 21 ppm, thereby bringing them into much better conformity with the experimental data. Since all aromatic nitrogens are in *ortho* or *para* positions relative to the NH_2 group in this series, analogy to the ^{13}C trends suggests that the inclusion of electron correlation effects would lead to more positive differences than those at the GIAO/SCF level. In fact, the ring nitrogen shifts of pyridine and 2-aminopyridine in Table 5 are the only exceptions (−13.6 and −3.4 ppm, respectively). However, even for these cases the differences in the DFT/STO-3G and SCF/STO-3G Mulliken $2p_z$ atomic populations (−0.0013 and −0.0045, respectively) are much less than those for any of the other nitrogens.

The importance of amine group conformational averaging to the ^{15}N NMR chemical shifts for the model compounds **3**, **8**, and **9** was examined by numerical integration using the computed chemical shifts $\delta(\mathrm{N}i,\varphi,\rho)$ and energies $\Delta E(\mathrm{N}i,\varphi,\rho)$ in eq 3. In Table 5, the differences between these averaged results $\langle\delta_i\rangle$ and those obtained at the minimum energy conformation δ_i are given in parentheses in the next to last column. By far the largest difference of −2.4 ppm occurs for the NH_2 group of aniline. However, the differences are less important for 4-aminopyrimidine (−0.6 ppm) and 2-aminopyrimidine (0.0 ppm), possibly because of the decrease in the computed inversion barriers. It is interesting to note that the computed −2.4 ppm increment would improve the agreement both for aniline and 1,3-diaminobenzene.

C. Proton Chemical Shifts. Entered in Table 6 are the calculated and experimental isotropic ^{1}H NMR chemical shifts for **1**−**12**. The calculated ^{1}H NMR chemical shifts $\delta_i(^1\mathrm{H})$ are also plotted in Figure 5 versus the experimental ^{1}H NMR chemical shifts for the 23 aromatic ring hydrogens for which experimental data appear to be available. The ^{1}H NMR chemical shifts also cover a substantial range from 4.7 to 9.3 ppm. Even though the inclusion of electron correlation effects does not improve the calculated ^{1}H NMR shifts as much as ^{13}C and ^{15}N NMR chemical shifts, only the GIAO/DFT results are included in Figure 5. Again, the solid line in the figure corresponds to unit slope and zero intercept.

On the much smaller scale for ^{1}H NMR chemical shifts, calculated results at the three DFT/GIAO levels are clearly delineated in Figure 5: $\delta(\mathrm{B{**}M{*}}) > \delta(\mathrm{B{**}B{*}}) > \delta(\mathrm{B{*}B{*}})$. The best correspondence between the calculated results and the experimental data does occur with inclusion of polarization functions at the B**B* level, represented by open triangles in Figure 5. Linear regression analyses for these data lead to

$$\delta(\mathrm{B{**}B{*}}) = 1.09\delta_{\mathrm{exp}} - 0.63\ \mathrm{ppm}$$

where r^2 is 0.974 and the standard deviation is 0.22 ppm. Comparisons of the results in Figure 5 with those for ^{13}C and

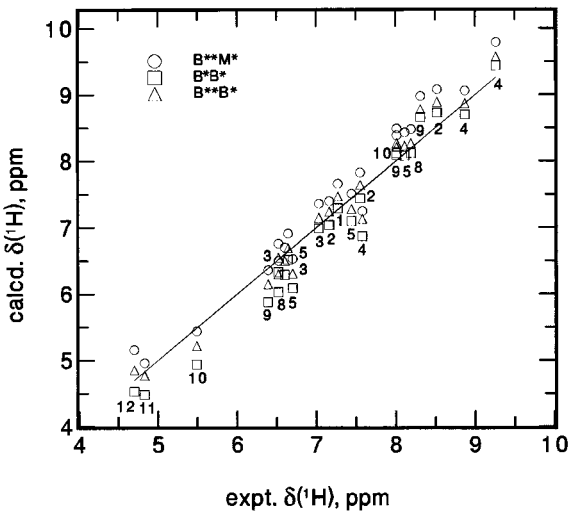

Figure 5. The calculated ^{1}H NMR chemical shifts are plotted versus experimental data from Table 5. Calculated results obtained at the B**M* level (○), at the B*B* level (□), and at the B**B* level (△). The solid line has unit slope and zero intercept.

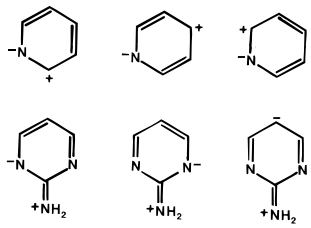

Figure 6. (a) Ionic valence bond structures for pyridine. (b) Ionic valence bond structures for 2-aminopyrimidine.

^{15}N in the previous two figures clearly show why computed ^{1}H NMR chemical shifts are often omitted in studies such as these. If we consider the ratio of the standard deviation to the chemical shift range to be a measure of the "resolution" of the computational method, the ^{13}C and ^{15}N NMR results are two to three times better "resolved" than the ^{1}H NMR results. Since the protons are on the periphery of the molecule, the ^{1}H NMR shifts are relatively more sensitive to solvent effects than the ^{13}C NMR shifts.

The persistent trends noted for ^{13}C and ^{15}N NMR shifts in this series of molecules follow for the ^{1}H NMR shifts but are an order of magnitude smaller, e.g., the B**M* results do not differ very much from B*B* because the inclusion of polarization functions (average +0.20 ppm) almost completely cancels the use of DFT geometry optimization (average −0.21 ppm) instead of MP2 optimization. Changes in the proton NMR chemical shifts in Table 6 on including electron correlation are positive (average 0.26 ppm) for hydrogens at *ortho* and *para* carbons and negative (average −0.10 ppm) for hydrogens at *meta* carbons.

V. Correlation of Chemical Shifts with 2p$_z$ Electron Densities

Because of the greater electronegativity of nitrogen, its presence in an aromatic ring leads to several ionic valence bond (VB) structures which will contribute to the ground state wave function. Those for pyridine depicted in Figure 6a produce charge separation between adjacent ring positions which will be enhanced by further nitrogen substitutions at the odd-numbered ring positions. The substitution of an amine group at the even-numbered ring carbons leads to additional ionic VB structures which will have the effect of increasing the *2*p$_z$ electron densities at the odd-numbered positions of the aromatic ring. For 2-aminopyrimidine, these structures are depicted in Figure 6b. To investigate these qualitative observations regarding progressive nitrogen substitutions, Mulliken populations for **1**−**12** were obtained at the BPW91/STO-3G level. Despite the warnings on the use of Mulliken populations,[69−71] these seem to behave well in these systems. The minimal STO-3G basis set results are simplistic, but are sufficient to provide fairly good correlations and trends in this study. In Figure 7, the *2*p$_z$ electron populations at the six ring positions are plotted as a function of the number of replaced nitrogens for the series benzene, pyridine, pyrimidine, 2-aminopyrimidine, 4,6-diaminopyrimidine, and 2,4,6-triaminopyrimidine. Figure 7 clearly shows that the 1, 3, and 5 positions undergo large monotonic increases in the *2*p$_z$ electron populations, while those at the 2, 4, and 6 positions change slightly. These trends qualitatively parallel the changes in the chemical shifts discussed in the previous sections.

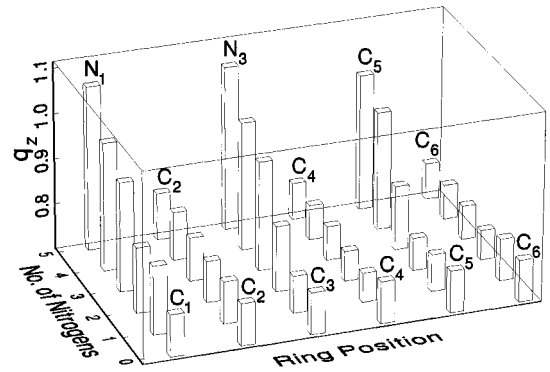

Figure 7. A bar graph showing the calculated *2*p$_z$ Mulliken populations at the six aromatic positions with progressive (0−5) nitrogen substitution: benzene, pyridine, pyrimidine, 2-aminopyrimidine, 4,6-diaminopyrimidine, and 2,4,6-triaminopyrimidine.

The correlation of chemical shifts with electron densities has long been a source of confusion because of the appearance of electron density in the diamagnetic term. However, changes in diamagnetic terms for carbon could not amount to more than a few ppm and the large chemical shifts changes noted here are associated with the way that changes in the *2*p$_z$ populations affect the (*xx* and *yy* components of the) paramagnetic term. This has been described previously by several authors.[3−6]

The calculated (open circles) and experimental (open squares) isotropic ^{13}C NMR chemical shifts $\delta(^{13}\mathrm{C})$ for all carbons at the *ortho* and *para* ring positions are plotted in Figure 8 as a function of the BPW91/STO-3G Mulliken *2*p$_z$ orbital populations q_z. The aminobenzenes **3**, **6**, and **7** were excluded. The linear regression of the experimental data

$$\delta(^{13}\mathrm{C}) = -233.4q_z + 308.3 \text{ ppm}$$

for which $r^2 = 0.973$ and the standard deviation is 3.4 ppm.

Plotted in Figure 9 versus the *2*p$_z$ Mulliken populations are the calculated and experimental isotropic ^{15}N NMR chemical shift data for the ring nitrogens of the pyridines and pyrimidines of this study. There is a fairly good relationship of the experimental data to the *2*p$_z$ Mulliken population

$$\delta(^{15}\mathrm{N}) = -509.7\, q_z + 353.1 \text{ ppm}$$

s where $r^2 = 0.956$ and the standard deviation is 9.8 ppm.

(70) Huzinaga, S.; Sakai, Y.; Miyoshi, E.; Narita, S. *J. Chem. Phys.* **1990**, *93*, 3319−3325.
(71) Bohmann, J.; Farrar, T. C. *J. Phys. Chem.* **1996**, *100*, 2646−2651.

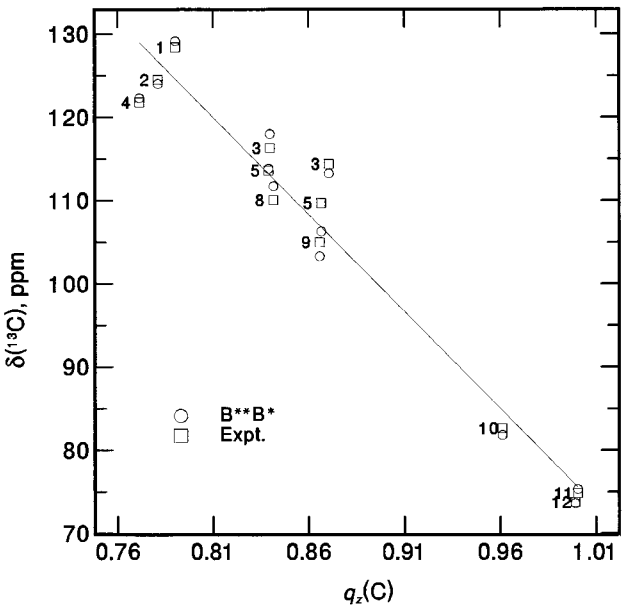

Figure 8. The calculated (○) and experimental (□) isotropic ^{13}C NMR chemical shifts $\delta(^{13}\mathrm{C})$ for all carbons at the *ortho* and *para* ring positions are plotted as a function of the BPW91/STO-3G Mulliken $2p_z$ orbital populations q_z(C).

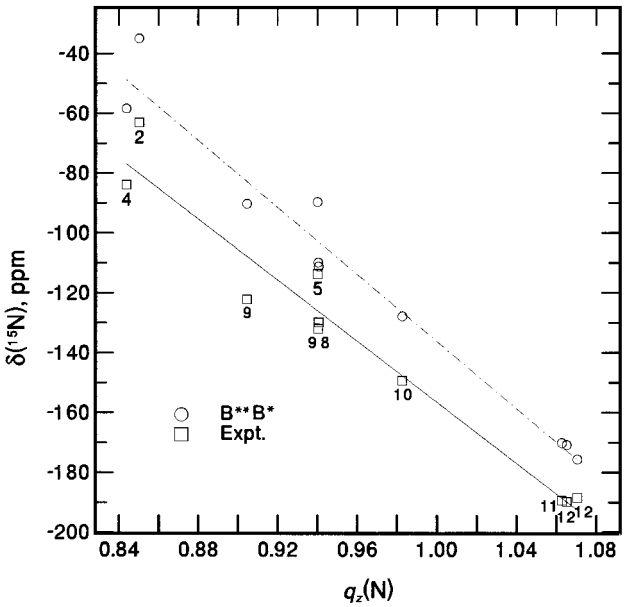

Figure 9. The calculated (○) and experimental (□) isotropic ^{15}N NMR chemical shift data for the ring nitrogens of the pyridines and pyrimidines of this study plotted as a function of the BPW91/STO-3G $2p_z$ Mulliken populations q_z(N).

VI. Dependencies of NMR Chemical Shifts and Electron Densities on Amine Group Orientation

Investigation of the importance of chemical shift averaging over the large amplitude amine group motions was of particular interest, since these must be reflected in the experimental values. Shielding calculations were performed for the model compounds aniline (**3**), 2-aminopyrimidine (**8**), and 4-aminopyrimidine (**9**). The NH_2 groups in these molecules are representative of the three local environments (-CH-CNH$_2$-CH-, -N-CNH$_2$-N-, and -CH-CNH$_2$-N-). Shielding computations for **3**, **8**, and **9** were performed at the B**B* level, analyzed via the truncated Fourier series of eq 2, and the results entered in Table 2. Because of the similarities in the conformational dependencies of the chemical shifts and electron densities, only those for 2-aminopyrimidine are described here. Data for the other two molecules are given in the Supporting Information.

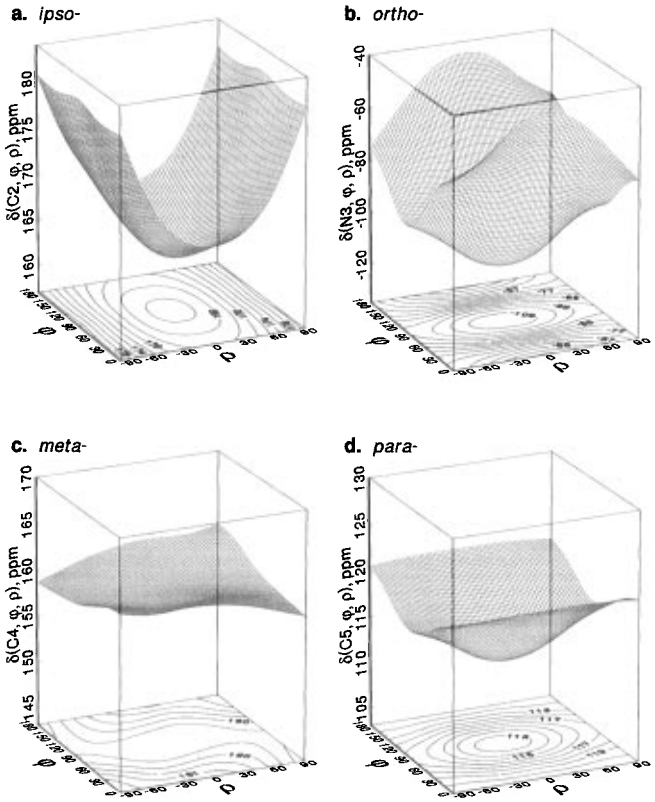

Figure 10. For the carbons and ring nitrogens of 2-aminopyrimidine (**8**), these are the surface and contour plots for calculated (B**B*) ^{13}C and ^{15}N NMR chemical shifts $\delta(\mathrm{C}i,\varphi,\rho)$ and $\delta(\mathrm{N}i,\varphi,\rho)$ as functions of the angles φ and ρ: (a) the C2 (*ipso*) carbon, the contour lines are separated by 2 ppm; (b) the N3 (*ortho*) nitrogen, the contour lines are separated by 5 ppm; (c) the C4 (*meta*) carbon, the contour lines are separated by 0.05 ppm; (d) the C5 (*para*) carbon, the contour lines are separated by 1 ppm.

Plotted in Figures 10a−d versus φ and ρ are surface and contour plots of the isotropic ^{13}C NMR chemical shifts $\delta(\mathrm{C}i,\varphi,\rho)$ of the 2-aminopyrimidine ring carbons C2, C4, and C5 and δ-(N3,φ,ρ) for the N3 nitrogen. Corresponding plots for the C6 carbon and N1 nitrogen are mirror images of those for N3 and C4 in Figures 10b and 10c, respectively. Spline algorithms were used to interpolate points in the surface and contour plots at 5° intervals of the two angles. Since the angles φ, and ρ are plotted in the ranges from 0 to 180° and −90 to 90°, respectively, the planar arrangement (90°, 0°) corresponds to the midpoint along both axes. To compare the plots, ^{13}C and ^{15}N NMR chemical shifts were plotted over 27 and 90 ppm ranges, respectively. Thus, on this scale the isotropic ^{13}C NMR chemical shifts of the *meta* carbons in Figure 10c exhibit a slight dependence on amine group orientation. For these carbons in Table 2b, it can be seen that the coefficients of the trigonometric terms are less than 1 ppm. Much larger variations occur at the *ortho* nitrogens and *ipso* and *para* carbons, all of which are most shielded in the planar arrangements.

Presented in Figures 11a−d are surface and contour plots of $2p_z$ Mulliken populations $q_z(\mathrm{C}i,\varphi,\rho)$ for each of the ring positions of 2-aminopyrimidine as functions of the two angles. For simplicity in the correlations with electron densities, the $2p_z$ Mulliken populations were evaluated at the BPW91/STO-3G level. At the *ipso* carbon, the shielding contours appear to be unrelated to the Mulliken populations in Figures 10a and 11a, respectively. This is also true for the ^{13}C NMR shifts and $2p_z$ populations at the *meta* carbon positions in Figures 10c and

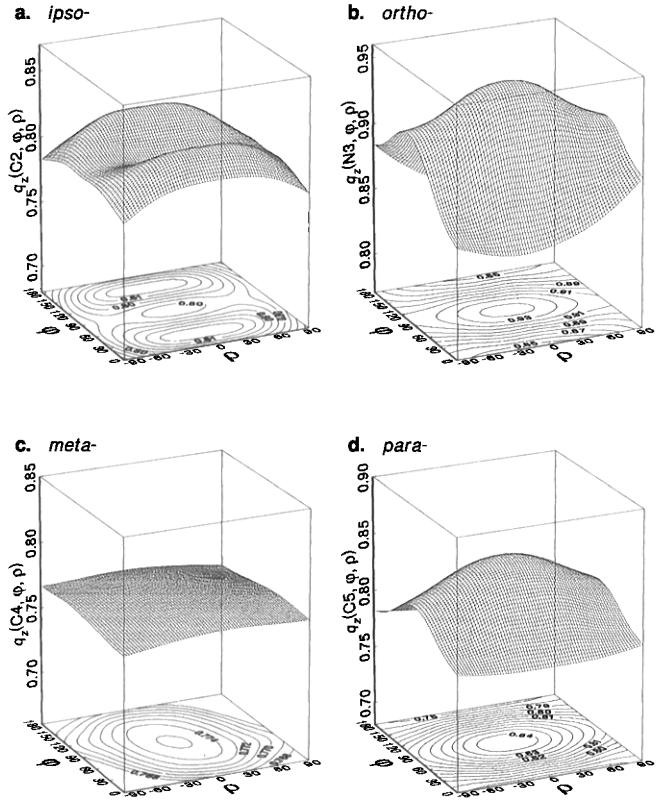

Figure 11. Calculated (BPW91/STO-3G//BPW91/6-311G*) surface and contour plots for the $2p_z$ Mulliken populations at the carbons q_z(Ci,φ,ρ) and ring nitrogens q_z(N3,φ,ρ) of 2-aminopyrimidine (**8**) plotted as a function of the angles φ and ρ: a) the C2 (*ipso*) carbon, the contour lines are separated by 0.005; (b) the N3 (*ortho*) nitrogen, the contour lines are separated by 0.010; (c) the C4 (*meta*) carbon, the contour lines are separated by 0.001; (d) the C5 (*para*) carbon, the contour lines are separated by 0.005.

11c, but the variations in both quantities are small. However, the contour plots of these quantities at the *ortho* nitrogens in Figures 10b and 11b are similar. In fact, linear regression of the nitrogen shifts δ(N3,φ,ρ) with the Mulliken populations q_z(N3,φ,ρ) at the *ortho* position leads to a fairly good correspondence between the two sets of data

$$\delta(\mathrm{N3},\varphi,\rho) = -626.3q_z(\mathrm{N2},\varphi,\rho) + 480.0 \text{ ppm}$$

where $r^2 = 0.963$ and 3.6 ppm standard deviation. At the *para* carbon position the contours are very similar in Figures 10d and 11d. Linear regression leads to

$$\delta(\mathrm{C5},\varphi,\rho) = -119.7q_z(\mathrm{C5},\varphi,\rho) + 214.1 \text{ ppm}$$

where $r^2 = 0.990$ and a standard deviation of only 0.2 ppm. This very good correlation of the calculated ^{13}C NMR chemical shifts with q_z at the *para* carbon position also extends to the ^{1}H NMR chemical shifts for the H5 proton

$$\delta(\mathrm{H5},\varphi,\rho) = -9.57q_z(\mathrm{C5},\varphi,\rho) + 14.39 \text{ ppm}$$

with $r^2 = 0.985$ and 0.02 ppm standard deviation.

VII. Conclusions

Progressive nitrogen replacement of benzene atoms (e.g., at C1, C3, H2, H4, and H6) produces changes in the ^{13}C, ^{15}N, and ^{1}H isotropic NMR chemical shifts, which represent large fractions of the total shift ranges for these nuclei. For example, the ^{13}C NMR resonances of 2,4,6-triaminopyrimidine and desoxyminoxidil cover ranges of 90 ppm and the ring nitrogens are more shielded than those of pyrimidine by 105 ppm. The calculated isotropic chemical shifts based on DFT/GIAO methods are in good agreement with the experimental results. The most dramatic changes in the ^{13}C and ^{15}N NMR chemical shifts on progressive nitrogen substitutions occur at *ortho* and *para* ring positions and parallel the changes produced in the $2p_z$ electron populations at these positions. The relative constancy of chemical shifts of *meta* carbons also parallels the small changes in electron populations at these atoms.

Comparisons of the GIAO/DFT and GIAO/SCF chemical shifts clearly show that electron correlation effects increase in importance with each additional NH_2 group. This has the effect of reducing the separations between chemical shifts for the *ortho*, *para* ring positions and the *ipso*, *meta* ring atoms and also parallels the decrease of the $2p_z$ electron densities at adjacent atoms on including electron correlation effects.

Both calculated and experimental results show that amine groups are tilted away from the ring plane by ca. 25−45°. Calculated results for the model compounds aniline, 2-aminopyrimidine, and 4-aminopyrimidine as functions of the orientation of the amine group indicate that the chemical shifts increase (less shielding) as the amine groups are moved away from the planar orientations with the largest changes occurring at the *ipso*, *ortho* and *para* ring positions. Since the largest change found on averaging the chemical shifts with respect to the energy profiles is −2.4 ppm for the nitrogen of aniline, it appears that this is not a very important factor in determining the shifts of aromatic amines.

Acknowledgment is extended to the National Science Foundation for partial support to purchase the IBM workstations used in this study. The assistance of Mrs. Susan Yamamura with computer related problems is greatly appreciated.

Supporting Information Available: Table presenting the structures for compounds **6**−**11** energy optimized at the MP2/6-311G* and BPW91/6-311G* levels and **12** at the MP2/6-31G* and BPW91/6-31G* levels, table presenting the averages of the ^{13}C and ^{15}N NMR shifts over the torsion and inversion coordinates at the HF/6-311G*//MP2/6-311G*, BPW91/6-311G**//MP2/6-311G*, and BPW91/6-311G**//BPW91/6-311G* levels for aniline and 2-amino- and 4-aminopyrimidine, and surface/contour plots of chemical shifts and $2p_z$ Mulliken populations for aniline and 4-aminopyrimidine (15 pages). See any current masthead page for ordering and Internet access instructions.

JA970990X